Fluorescence Anisotropy Studies of Enzyme−Substrate Complex Formation in Stearoyl-ACP Desaturase†

Jeffrey A. Haas‡ and Brian G. Fox*

Department of Biochemistry, College of Agricultural and Life Sciences, University of Wisconsin, Madison, Wisconsin 53706

Received May 7, 2002

ABSTRACT: Stearoyl-acyl carrier protein Δ^9-desaturase (Δ9D) catalyzes regio- and stereospecific insertion of *cis* double bonds into acyl chains attached to acyl carrier protein. Steady-state and stopped-flow fluorescence anisotropy measurements using acylated forms of dansyl- and fluoresceinyl-ACPs revealed equilibrium dissociation constants and dissociation rate constants for 16:0-, 17:0-, and 18:0-ACPs with resting and chemically 4e$^-$ reduced Δ9D. Binding of 1 nM 18:0-fluoresceinyl-ACP to one subunit of the dimeric resting Δ9D was observed with $K_{D1} = 13 \pm 3$ nM. No significant difference in the K_{D1} value was observed for 4e$^-$ Δ9D. An ∼4-fold increase in K_{D1} per methylene group was observed upon shortening the acyl chain from 18:0 to 17:0 and then 16:0. In different experiments performed with 850 nM 18:0-dansyl-ACP, binding to the second subunit of resting Δ9D was estimated to have $K_{D2} \approx 350 \pm 40$ nM. The K_{D2} values exhibited a similar dependence on acyl chain length as observed for the K_{D1} values. The k_{off} values measured by stopped-flow anisotropy measurements for reversal of the enzyme−substrate complex were also acyl-chain length dependent and increased 130-fold for 16:0-ACP (130 s^{-1}) relative to 18:0-ACP (1 s^{-1}). Increases in acyl chain length are thus associated with the presently reported increases in the K_D and k_{off} values. These results indicate that acyl chain length selectivity derives in major part from partition of the enzyme−substrate complex between substrate release and subsequent steps in catalysis.

The soluble acyl-ACP[1] Δ^9-desaturases catalyze the insertion of *cis* double bonds into fatty acids that are covalently attached by a thioester linkage to the 4′-phosphopantetheine prosthetic group of ACP. These enzymes are found in photoauxotrophic *Euglena*, in the plastid organelles of plants, and possibly in some Gram-positive bacteria and filamentous fungi (*1*−*3*). The soluble desaturases are members of a structurally related family of diiron enzymes (*4*−*8*) that also includes the R2 component of ribonucleotide diphosphate reductase (*9*) and bacterial hydrocarbon monooxygenases (*10*). These diiron enzymes are related by the presence of two copies of a conserved iron binding sequence motif (D/E)$X_{\sim 40}EX_2H$ separated by ∼100 amino acids (*6*). Furthermore, the above-mentioned enzymes all bind and activate O_2 as part of their respective catalytic cycles, and related oxidized intermediates of the diiron center have been proposed and characterized (*11*).

The castor (*Ricinus communis*) Δ9D is the best physically characterized member of the subfamily of soluble acyl-ACP desaturases (*6*, *12*−*16*). Δ9D inserts a double bond between the C-9 and C-10 positions of the acyl chains in *n*:0-ACPs to exclusively give *cis*-Δ^9-*n*:1-ACPs, with 18:0-ACP serving as the kinetically preferred substrate (*17*). Each subunit of the ∼84 kDa α_2-desaturase holoenzyme contains a diiron center that is utilized for the O_2 activation steps of catalysis (*6*, *18*). In plants, naturally occurring variants of the acyl-ACP desaturases share high amino acid sequence identity (>70%, including conservation of all ligands to the diiron center) while also exhibiting selectivities for shorter chain acyl-ACPs and different specificities for the position of double bond insertion (*5*). The X-ray structure of Δ9D showed that the diiron center was buried within the protein and along a tunnel with appropriate dimensions for binding a C_{18} fatty acid (*12*). Mutations that blocked the distal end of the channel resulted in increased desaturation of a C_{16} fatty acid (*19*), implying that steric interactions play an important role in acyl chain length selectivity. Spectroscopic studies have reinforced the importance of interactions between acyl-ACP and Δ9D during catalysis, as the accumulation of a quasi-stable peroxodiiron(III) species (*14*, *16*), the alteration of the ligation environment of the diferrous center (*15*), and the stimulation of the rate of reaction between the diferrous center and O_2 by ∼10^4-fold (*14*) all require the presence of a long-chain acyl-ACP. Furthermore, comparison of k_{cat}/K_M values indicated that the acyl chain

† This work was supported by National Institutes of Health Grant GM-50853 to B.G.F.

* To whom correspondence should be addressed. E-mail: bgfox@biochem.wisc.edu. Telephone: (608) 262-9708. Fax: (608) 265-2904.

‡ Trainee of the NIH Institutional Molecular Biophysics Pre-Doctoral Training Grant T32 GM-08293.

[1] Abbreviations: ACP, biologically active form of ACP containing phosphopantetheine; fACP, 3-aminotyrosyl-ACP containing fluorescein covalently attached to the ϵ-amino group of chemically derivatized Tyr71 of *Escherichia coli* ACP; dACP, ACP containing dansyl covalently attached as for fACP; *n*:0-ACP, ACP with an *n*-carbon saturated fatty acid covalently attached to ACP through a phosphopantetheine thioester bond; apo-ACP, form of ACP lacking phosphopantetheine; apo-fACP, 3-aminotyrosyl-ACP containing fluorescein covalently attached to the ϵ-amino group of chemically derivatized Tyr71 of *Escherichia coli* apo-ACP; Δ9D, 18:0-ACP Δ^9-desaturase; resting Δ9D, as-isolated form of Δ9D containing all ferric sites; 4e$^-$ Δ9D, reduced form of Δ9D containing all ferrous sites; E_2, an unbound dimer of Δ9D; AE_2, a complex of one acyl-ACP with E_2; AE_2A, a complex of two acyl-ACPs with E_2; Fd, *Anabaena* 7120 vegetative [2Fe-2S] ferredoxin; T4moD, 11.6 kDa effector protein of the toluene-4-monooxygenase complex.

10.1021/bi020340s CCC: $22.00 © 2002 American Chemical Society
Published on Web 11/14/2002

length selectivity arose from a systematic ~4-fold increase in k_{cat} per methylene group as the acyl chain length was increased from 14:0 to 19:0 (~115-fold increase), while the apparent K_M values showed only a nonsystematic 3-fold difference for this entire set of acyl chain lengths (*17*).

In light of the accumulating evidence for the contribution of the acyl chain and protein−protein interactions in various aspects of soluble desaturase catalysis, further examination of the kinetics and energetics of association between acyl-ACP and Δ9D is warranted. For example, an identification of individual binding and/or chemical steps that might give rise to acyl chain length selectivity has not yet been undertaken (*17*). Here we report the use of fluorescence anisotropy and a site-specifically modified *Escherichia coli* ACP (*20*) containing either dansyl or fluorescein as a catalytically silent label to study binding interactions between the acyl-ACPs and Δ9D. This approach has permitted the examination of equilibrium binding constants and dissociation rates for the resting Δ9D−substrate complex as a function of acyl chain length. The results show a tight binding of 18:0-ACP to one subunit of the dimeric resting enzyme and a 30-fold weaker binding of 18:0-ACP to the second subunit. The affinity for acyl-ACP was dependent on the length of the acyl chain, and importantly, a *decrease* in the acyl chain length was associated with an *increase* in the dissociation rate for the enzyme−substrate complex. These results more fully account for the acyl chain length selectivity characteristic of this enzyme.

MATERIALS AND METHODS

Reagents and Proteins. Recombinant *E. coli* ACP and castor Δ9D were expressed, purified, and characterized as previously described (*20*, *21*). In summary, apo-(3-amino-Tyr71)-ACP was produced from apo-ACP by reaction of the Tyr71 residue with tetranitromethane, followed by sodium dithionite-mediated reduction of the aromatic nitro group to the aromatic amine, and reaction of the aromatic amine with an activated fluorophore to give apo-dACP (*20*). The dACP and acyl-dACP derivatives were produced by in vitro enzyme modifications and characterized as previously described (*20*). The p*I* values of ACP, lysozyme, and T4moD were calculated from their amino acid sequences using the Protean module of the LaserGene Navigator (version 5.01, DNAStar, Madison, WI). In this work, the reported concentration of Δ9D corresponds to the monomer polypeptide concentration as determined by optical spectroscopy ($\epsilon_{340} = 4800$ M^{-1} cm^{-1} per diiron center).

Fluoresceinylation Reaction. The fluoresceinylation reaction was performed at 20 °C and contained 40 μM apo-(3-amino-Tyr71)-ACP (~35−40 mg) in 50 mM sodium acetate, pH 5.0, with 35% (v/v) dimethylformamide. Fluorescein isothiocyanate (Molecular Probes, Eugene, OR) was prepared as a 15 mM solution in dimethylformamide and was slowly added to the rapidly stirred reaction mixture to give a final concentration of 1.5 mM. The reaction was terminated after 1 h by the addition of 3-aminotyrosine in 50 mM sodium acetate buffer, pH 5.0, to give a final concentration of 50 mM 3-aminotyrosine. The apo-fACP was precipitated by the addition of dilute acetic acid to give a pH of ~3.9 and recovered by centrifugation. The resulting protein pellet was resuspended in 8 mL of 0.3 M MES, pH 6.1. Fluoresceinyl-3-aminotyrosine was removed from apo-fACP by gel filtration on a Sephadex G-15 (Pharmacia LKB Biotechnology Inc., Piscataway, NJ) column (25 mm i.d. × 7.5 mm bed height) equilibrated with 25 mM MES, pH 6.0, containing 0.15 M NaCl at a linear flow rate of ~12 cm h^{-1}. The column eluate containing apo-fACP was diluted with 25 mM MES, pH 6.0, to reduce the salt concentration to 0.05 M NaCl. The apo-fACP was further purified from apo-(difluoresceinyl)-ACP on a 16/10 HiLoad Q-Sepharose Fast Flow column (Pharmacia LKB Biotechnology Inc.). The column was loaded with apo-fACP at a linear flow rate of 15 cm h^{-1} in 25 mM MES, pH 6.0, washed with 100 mL of 25 mM MES, pH 6.0, and then washed with 100 mL of 25 mM MES, pH 6.0, containing 0.1 M NaCl. The protein was eluted at a linear flow rate of 15 cm h^{-1} in a 300 mL linear gradient from 0.05 to 0.7 M NaCl in 25 mM MES, pH 6.0. The purified apo-fACP was characterized by electrospray ionization mass spectrometry (8913 Da expected, 8912 Da observed).

Phosphopantetheinylation, Acylation, and Characterization of Acyl-fACP. In vitro phosphopantetheinylation and acylation were carried out as previously described (*20*) to produce acyl-fACPs in >98% yield starting from apo-fACP. Acyl-fACPs were hydrolyzed at alkaline pH, and the resulting free thiol in holo-fACP was quantitated with DTNB (*20*). Since the acylation reaction proceeded in high yield, the acyl-fACPs could also be quantitated by absorbance spectroscopy using the chromophore introduced by fluorescein [$\epsilon_{494} = 73000$ M^{-1} cm^{-1} (*22*)]. The concentrations of acyl-fACP determined by either the acyl chain cleavage/DTNB reaction or the fluorescein molar absorptivity were within experimental error of each other.

Equilibrium Fluorescence Anisotropy Measurements. For anisotropy measurements, the intensity of the parallel and perpendicular emission from a blank containing buffer and either resting or 4e$^-$ Δ9D as appropriate was subtracted from the corresponding intensity obtained from each sample. Anisotropy measurements were repeated five times for each sample, and the resulting values were averaged. The observed anisotropy, r, is defined in eq 1, where $I_{||}$ and $I_{\perp}$ are the parallel and perpendicular components of the fluorescence emission intensity (*23*). The total anisotropy was considered to be the sum of the intensity-weighted contributions of the individual anisotropies of the labeled ACP free in solution and in the various enzyme-bound forms.

$$r = (I_{||} - I_{\perp})/(I_{\perp} + 2I_{||}) \quad (1)$$

Fluorescence anisotropy titration measurements with *n*:0-fACP were carried out with a Beacon 2000 variable temperature fluorescence polarization system (PanVera Corp., Madison, WI) at 23 °C. The instrument was set to read six cycles, corresponding to an integration time of 16 s per measurement. Separate samples of *n*:0-fACP for each concentration of Δ9D were prepared for each titration data point by diluting the concentrated *n*:0-fACP to the desired final concentration in a total volume of 650 μL of 50 mM Hepes, pH 7.8, containing 35 mM NaCl (typically >10^4-fold dilution). An appropriate amount of resting Δ9D in the same buffer was added to each aliquot of *n*:0-fACP to give the desired final concentration of Δ9D with less than a 5% increase in volume for each aliquot. The final concentration of *n*:0-fACP was ~1 nM. As indicated for certain experi-

ments, either NaCl or Fd was added to the titration buffer to give a final concentration of either 0.2 M or 3 μM, respectively.

Fluorescence anisotropy measurements using 18:0-dACP were made at 23 °C on an OLIS-RSM 1000F spectrophotometer that was modified for the measurement of fluorescence anisotropy in T-format. Each photomultiplier tube was fitted with a glass long-pass 500 nm cutoff filter (Oriel, Stratford, CT) and either a vertical or a horizontal quartz polarizer. A 450 W Xe arc lamp with a single grating monochromator was used for excitation of 18:0-dACP with 335 nm light. Samples of *n*:0-dACP for each concentration of Δ9D were prepared as described above for *n*:0-fACP, except that the sample aliquot was 650 μL of 50 mM Hepes, pH 7.8, containing 35 mM NaCl, and the final concentration of *n*:0-fACP was 850 nM. An appropriate amount of resting Δ9D was added to each aliquot of 18:0-dACP to give the desired final concentration of Δ9D with less than a 5% increase in volume for each aliquot.

Binding Analyses. The data from equilibrium binding titrations of *n*:0-fACPs were analyzed by nonlinear least-squares fitting using Kaleidagraph (Synergy Software, West Palm Beach, FL) and eq 2, which accounts for the anisotropy contributions of two independent classes of binding sites and the contribution of unbound acyl-fACP (*24*). In eq 2, r is

$$r = \frac{(r_{bound} - r_{free})[\Delta 9D_{tot}]}{K_{D1} + [\Delta 9D_{tot}]} + \frac{(r_{non} - r_{free})[\Delta 9D_{tot}]}{K_{non} + [\Delta 9D_{tot}]} + r_{free} \quad (2)$$

the observed anisotropy, r_{free} is the anisotropy value of either free apo- or free acyl-fACP, r_{bound} is the anisotropy value of *n*:0-fACP bound to a Δ9D subunit in the nanomolar concentration range, K_{D1} is the dissociation constant for complex formation in the nanomolar concentration range, r_{non} is the anisotropy value observed for an electrostatic complex formed when the total Δ9D concentration was in excess of ~5 μM, and K_{non} is the dissociation constant for this complex. The r_{free} values were obtained from experimental measurements and used as constants in subsequent data analysis, while r_{bound}, r_{non}, K_{D1}, and K_{non} were given by the fitting routine. For 18:0-fACP, $r_{free} = 0.098$, $r_{bound} = 0.130$, and $r_{non} = 0.203$. Overall similar values were obtained for the other acyl chain lengths. For the *n*:0-fACP titration experiments, the concentration of *n*:0-fACP was at least 10-fold lower than K_{D1}. The free concentration of Δ9D upon complete complexation of 16:0-fACP (the least tightly bound substrate; see below) was ill-defined due to an overall similarity between the concentration required for saturation of the acyl chain-dependent specific interaction and the onset of electrostatic binding interactions associated with K_{non}. However, correction of the total Δ9D concentration for the fraction bound to 18:0-fACP resulted in changes to the K_{D1} values that were within error from those derived from fitting the uncorrected total Δ9D concentration data. Therefore, for consistency, the reported K_{D1} values for 16:0-, 17:0-, and 18:0-fACPs were all obtained from fits to the change in anisotropy versus total Δ9D concentration only.

The data from titrations of *n*:0-dACPs were analyzed by using eqs 3−6 and the NSolve routine (Mathematica 4.0.1.0, Wolfram Research, Inc., Champaign, IL). The NSolve routine calculated the individual concentrations of all enzyme and substrate species present during the progress of the titration experiments as a function of the independent variables K_{D1} and K_{D2}.

$$[E_{2,total}] = [E_{2,free}] + [AE_2] + [AE_2A] \quad (3)$$

$$[A_{total}] = [A_{free}] + [AE_2] + 2[AE_2A] \quad (4)$$

$$K_{D1} = ([E_{2,free}][A_{free}])/[AE_2] \quad (5)$$

$$K_{D2} = ([AE_2][A_{free}])/[AE_2A] \quad (6)$$

The concentration values provided by the NSolve routine were used to calculate predicted total anisotropy values from the following experimentally determined end point anisotropy values: 0.112 for unbound acyl-dACP (r_{free}) and 0.22 for the complex containing one acyl-dACP bound to the Δ9D dimer (AE_2; note that the large excess of Δ9D present at the end of the titration ensures formation of AE_2, not AE_2A). An estimated value of 0.225 was used for the complex containing two acyl-fACPs bound to the Δ9D dimer (AE_2A) based on the anticipated mass change from AE_2 to AE_2A. The K_D values were further refined using the NSolve routine by minimization of the normalized square of the residuals between the calculated and observed anisotropy values as defined by eq 7.

$$\sum(r_{calcd} - r_{obsd})^2/\sum(r_{obsd})^2 \quad (7)$$

Time-Resolved Fluorescence Anisotropy Measurements. These measurements were made with an SX.18M stopped-flow spectrophotometer equipped with an FP.1 fluorescence polarization modification (Applied Photophysics, Leatherhead, U.K.). The instrument was configured in T-format, and emission was collected through Schott OG-530 glass cutoff filters (Oriel, Stratford, CT) placed in front of each photomultiplier tube. To determine k_{off} from Δ9D for each of the *n*:0-fACPs, one syringe was loaded with 0.2 μM *n*:0-fACP and 2 μM Δ9D that had been allowed to equilibrate for 5 min at 23 °C in 50 mM Hepes, pH 7.8, containing 35 mM NaCl. The other syringe was loaded with either buffer (control experiment) or with 20 μM 18:0-ACP in the same buffer that was not labeled in order to provide a competition binding experiment. After rapid mixing, the final concentrations in the flow cell were 0.1 μM *n*:0-fACP, 1 μM Δ9D, and, when present, 10 μM 18:0-ACP. Data were collected in an oversampling mode with 1000 points collected per rapid-mix shot. For each *n*:0-fACP, the data from five consecutive shots were averaged and smoothed using software provided with the instrument. The data were fit to a single-exponential decay with the Levenberg−Marquardt algorithm provided in Kaleidagraph. The errors reported for the k_{off} values were derived from the fitting procedures.

Preparation of Samples Containing 4e⁻ Δ9D. Fluorescence anisotropy measurements using fACP and 4e⁻ Δ9D were performed in sample tubes fitted with a rubber septum stopper. Each stoppered sample was prepared with 1 nM *n*:0-fACP in 50 mM Hepes, pH 7.8, containing 35 mM NaCl and made anaerobic by repeated cycling between vacuum and back-fill with O_2-free Ar. An appropriate amount of 4e⁻ Δ9D was transferred under Ar to each aliquot of *n*:0-fACP

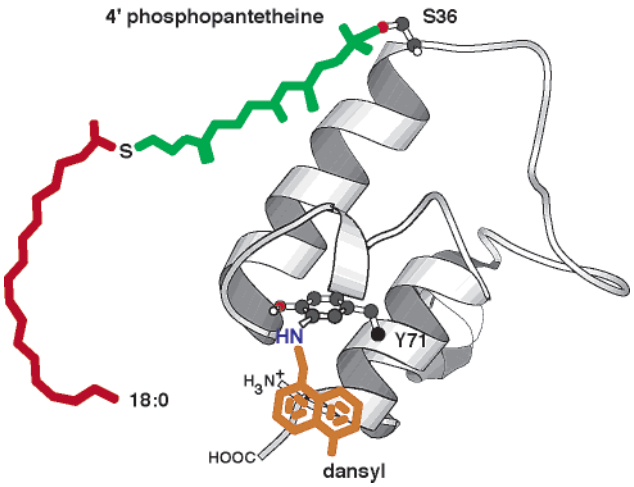

FIGURE 1: Depiction of 18:0-dansyl-ACP derived from the NMR structure of *Escherichia coli* apo-ACP (*28*) showing the locations of the key residues Ser36 and Tyr71. The phosphopantetheine (green), acyl chain (red), and dansyl (orange) groups present in the complete substrate molecule are not structurally defined but included for illustrative purposes.

to give the desired final concentration of Δ9D. The 4e$^-$ Δ9D was prepared from a solution containing 32 μM resting Δ9D and 2 μM Fd in 50 mM Hepes, pH 7.8, containing 35 mM NaCl. This solution was made anaerobic by repeated cycling between vacuum and back-fill with O_2-free Ar. The resting Δ9D was reduced by titration with 0.15 M sodium dithionite prepared in anaerobic 1 M potassium phosphate buffer, pH 7.0, using Fd as the electron transfer mediator. Following reduction, the solution was serially diluted into anaerobic buffer under Ar to produce stock solutions containing either 3.2, 0.32, or 0.032 μM 4e$^-$ Δ9D.

RESULTS

Strategy for Fluorescent Labeling of ACP. We considered that an important prerequisite for these studies would be the introduction of a fluorophore that would not perturb either productive binding or catalysis. Early studies of *E. coli* ACP using the methods of proteolytic digestion and chemical modification showed the importance of the N-terminal region for ACP function but also implied that the C-terminal region might be modified without affecting function (*25*, *26*). This suggestion was supported by our previous demonstration of the kinetic competence of spinach ACP containing a C-terminal His_6 tag (*27*). Therefore, our derivatization strategy targeted Tyr71, which is the only Tyr residue present in *E. coli* ACP and which is located near to the C-terminus (*20*). Figure 1 gives a illustrative representation of 18:0-dACP, based on the NMR structure determined for *E. coli* apo-ACP (*28*), and includes the sites of phosphopantetheinylation (Ser36), acylation (phosphopantetheine thiol group), and dansylation (3-amino-Tyr71) required to create the substrates used in this work. Initial studies with 18:0-dACP showed no changes in fluorescence intensity in static binding experiments in the presence of resting Δ9D in the concentration range of 1 nM to 1 μM, which was consistent with our initial objective. Furthermore, no evidence for a change in fluorescence intensity of the bound fluorophore was obtained by use of plotting estimation approaches (*29*, *30*).

Catalytic Properties of Acylfluoresceinyl-ACPs. Following minor adjustments to our chemical modification protocols

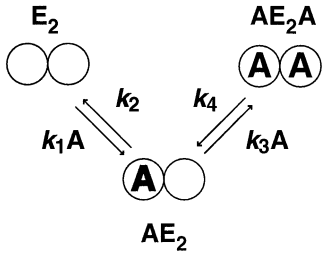

FIGURE 2: Binding equilibria considered in this work. Circles represent individual subunits of dimeric Δ9D; A, *n*:0-ACP substrate; $K_{D1} = k_2/k_1A$; and $K_{D2} = k_4/k_3A$.

(*20*), apo-fACP was synthesized on the milligram scale (10−50 mg yield of apo-fACP, >25% recovery relative to starting apo-ACP). Apo-fACP gave equivalent behavior to the natural protein during the in vitro phosphopantetheinylation and acylation reactions and also permitted efficient, high-yield attachment of acyl chains. Importantly, the acyl-fACPs were comparable to the unmodified acyl-ACPs as judged by steady-state kinetic analysis of their desaturation by Δ9D, which revealed $k_{cat} = 20$ min^{-1} and $K_M = 2.2$ μM for desaturation of 18:0-fACP to 18:1-fACP. Furthermore, the $k_{cat}/K_M = 9$ μM^{-1} min^{-1} determined for 18:0-fACP was close to the 10 μM^{-1} min^{-1} previously reported for 18:0 forms of ACP, dACP, and spinach ACP-His_6 (*17*, *20*). These results establish the efficacy of 18:0-fACP and 18:0-dACP as catalytically silent probes for studies of the binding to Δ9D and the subsequent desaturation reaction.

Binding Interactions with Acyl-fACP. Δ9D is a homodimeric enzyme potentially capable of productively binding one acyl-ACP per subunit. In the following, the unbound dimer of Δ9D will be referred to as E_2, the complex of one acyl-ACP with E_2 as AE_2, and the complex of two acyl-ACPs with E_2 as AE_2A. These enzyme states and abbreviations are shown in Figure 2, which also provides a schematic representation of the binding equilibrium that is considered in this work.

Acyl Chain Length Dependence of Equilibrium Dissociation Constants. For all experiments involving fACP derivatives, the total fluorescence intensity varied in a nonsystematic manner within 0.2−6% and showed no other variations during the progress of the titration with either Δ9D or other control proteins investigated below. Figure 3A shows anisotropy data from titrations of either 18:0-fACP (solid triangles) or apo-fACP (open triangles) with resting Δ9D. Figure 3B shows the anisotropy data obtained from titrations of ~1 nM 16:0-, 17:0-, and 18:0-fACP with resting Δ9D. A comparison of these titration results showed that the presence of an acyl chain was required for tight binding. Furthermore, the results revealed that the affinity of the complex formed in the presence of an acyl chain was dependent on the length of the acyl chain. The solid lines of Figure 3 were obtained from nonlinear least-squares fitting using the two binding site model of eq 2, which accounts for an acyl chain-dependent tight-binding interaction and an independent, weaker binding interaction observed when the concentration of Δ9D exceeded ~5 μM. Table 1 shows the K_{D1} values obtained for 16:0-, 17:0-, and 18:0-fACP from these fitting procedures. In the experiments of Figure 3, the low amount of acyl-fACP present effectively limited binding interactions to the occupation of a single subunit of dimeric Δ9D, corresponding to the equilibrium between E_2 and AE_2

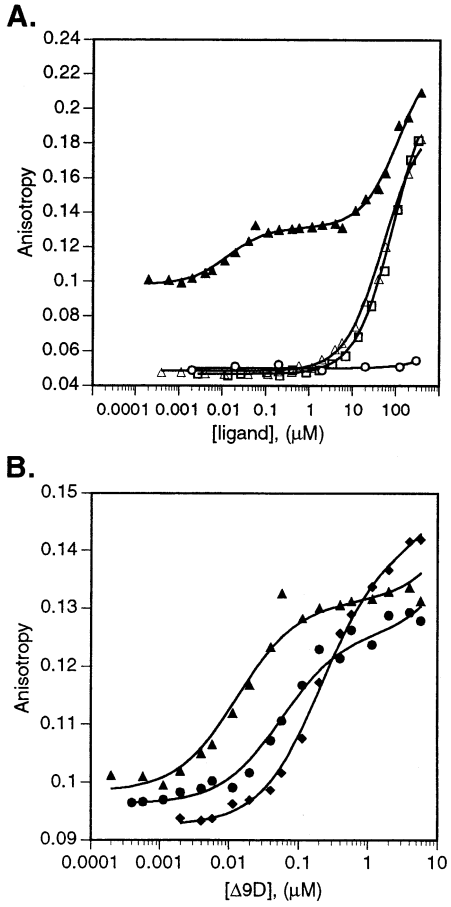

FIGURE 3: Fluorescence anisotropy changes observed during titration of *n*:0-fACPs with various protein ligands. (A) 1 nM 18:0-fACP with resting Δ9D (▲), 0.97 nM apo-fACP with resting Δ9D (△), 0.97 nM apo-fACP with lysozyme (□), and 0.97 nM apo-fACP with T4moD (○). (B) Titration of 1 nM 18:0-fACP (▲), 0.7 nM 17:0-fACP (●), and 1.3 nM 16:0-fACP (◆) with resting Δ9D. Solid lines are the results of nonlinear least-squares fitting using eq 2 as described in Materials and Methods.

Table 1: Comparison of K_D Constants, Rates, and Steady-State Kinetic Parameters for Various Acyl-ACPs and Resting and $4e^-$ Δ9D

	K_{D1}[a] × 10^6 (M)	K_{D2}[b] × 10^6 (M)	k_{off}[c] (s^{-1})	k_{cat}/K_M[d] ($\mu M^{-1}\ s^{-1}$)
resting Δ9D				
18:0	0.013 (0.0034)	0.35 (0.040)	1.0 (0.026)	10
17:0	0.057 (0.010)	0.76 (0.059)	49 (4.2)	2.5
16:0	0.21 (0.016)	0.95 (0.076)	130 (9.3)	0.69
$4e^-$ Δ9D				
18:0	0.011 (0.0033)			

[a] Dissociation constants expressed relative to the Δ9D active site concentration from nonlinear least-squares fitting as described in Materials and Methods. K_{D1} values from fluorescence anisotropy using ~1 nM *n*:0-fACP. [b] K_{D2} values from fluorescence anisotropy using ~850 nM *n*:0-dACPs and NSolve evaluation of the titration data. [c] Substrate dissociation rate measured from relaxation of a preformed complex of *n*:0-fACP and Δ9D in the presence of excess 18:0-ACP by stopped-flow fluorescence anisotropy. The measured k_{off} values may correspond to k_2, k_4, or both as elaborated in the Discussion. [d] The k_{cat}/K_M values were from ref *17*.

assigned to K_{D1} in Figure 2. For each methylene group added to an acyl chain of length of 16:0 to 18:0, an ~4-fold increase in the affinity of the complex with resting Δ9D was obtained as reflected in changes in K_{D1}. The results also show that 18:0-fACP was the most tightly bound substrate tested, with $K_{D1} = 13$ nM.

For studies of 18:0-fACP binding to $4e^-$ Δ9D, an O_2-free preparation of resting Δ9D was first reduced in the presence of a substoichiometric amount of Fd as the redox mediator and sodium dithionite as the reducing agent. The reductive titration was monitored by optical spectroscopy at 350 nm and indicated that greater than 95% reduction of the diiron centers was achieved. A titration of O_2-free 18:0-fACP using these preparations of $4e^-$ Δ9D gave a K_{D1} value indistinguishable from that measured for the complex with resting Δ9D (Table 1). This result suggested that major changes in the affinity for acyl-ACP would not be produced as result of redox transformations of the Δ9D diiron center. Therefore, further investigations of the binding interactions with $4e^-$ Δ9D were not undertaken in this work.

Electrostatic Contributions to Nonspecific Binding. Although the results of Figure 3A indicated that tight binding between acyl-fACP and resting Δ9D was dependent upon the presence of an acyl chain, a second binding interaction was also observed at the higher concentrations of Δ9D tested. This second binding interaction was independent of the presence of an acyl chain as titration of apo-fACP with resting Δ9D gave a change in anisotropy, but only when the added Δ9D concentration exceeded ~5 μM (Figure 3A, open triangles). Likewise, titration of apo-fACP (pI = 3.8, net negative charge at sample pH) with lysozyme (pI = 8.6, net positive charge) gave no change in anisotropy in the nanomolar concentration regime but gave a substantial change in anisotropy in the micromolar concentration regime (Figure 3A, open squares). In contrast, titration of apo-fACP with T4moD (pI = 4.4, net negative charge) produced only a small anisotropy change ($\Delta r \approx 0.005$) over the entire concentration range investigated (Figure 3A, open circles). These results suggest that the anisotropy changes observed from both apo- and acyl-fACPs in the presence of micromolar concentrations of either Δ9D or lysozyme arise from electrostatic interactions. Since the surface of Δ9D has many positively and negatively charged amino acids, we propose that the binding equilibrium observed from Δ9D concentrations of ~5 μM and above may thus arise from electrostatic interactions between an already formed AE_2 complex and excess Δ9D.

Binding Interactions with 18:0-Dansyl-ACP. The dansyl fluorophore has a lower quantum yield than fluorescein (*22*), which allows the use of higher concentrations of the labeled substrate in binding investigations. Therefore, these experiments provided insight into K_{D2}, the equilibrium between AE_2 and AE_2A. Titration of 850 nM 18:0-dACP with Δ9D showed that all 18:0-dACP was bound when an equivalent concentration of 18:0-dACP and the subunits of dimeric Δ9D was attained (Figure 4A). This result implies tight, stoichiometric binding. Figure 4B, solid line, shows a nonlinear least-squares evaluation of the anisotropy data derived from eqs 3−6 assuming two inequivalent binding interactions with K_{D1} = 13 nM (as determined from the measurements of Figure 3B with 18:0-fACP) and K_{D2} = 350 nM (optimized as an independent variable on the basis of the goodness-of-fit values calculated using eq 7). For comparison, illustrative fits assuming $K_{D1} = K_{D2} = 13$ nM (dotted line) or $K_{D1} = K_{D2} = 350$ nM (dashed line) as lower and upper limits, respectively, gave an inadequate simulation on the basis of

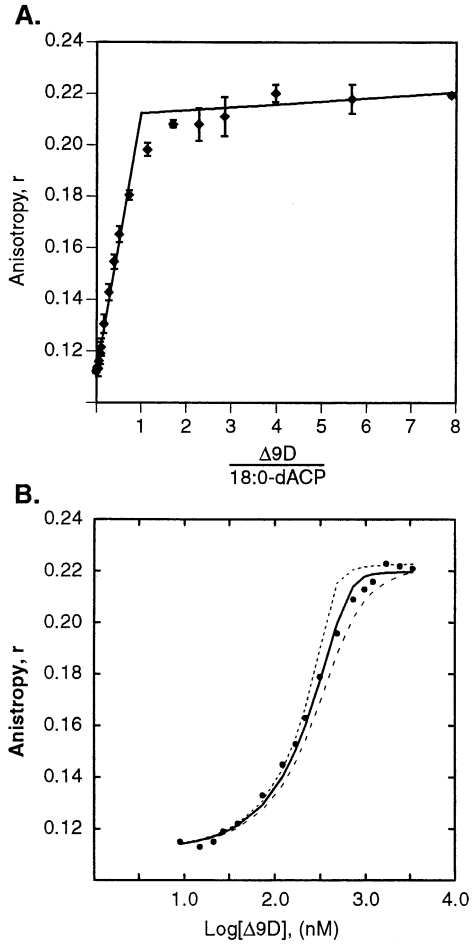

FIGURE 4: Fluorescence anisotropy changes observed during titration of 18:0-dACP with resting Δ9D. (A) Titration of 850 nM 18:0-dACP with Δ9D showing a 1:1 stoichiometry of binding. The solid lines are linear least-squares fits to the linear portions of the titration data below and above the apparent stoichiometric break point. (B) Binding analysis of the titration data from (A). Fitting results were derived from eqs 3−6 as described in Materials and Methods assuming $K_{D1} = 13$ nM and $K_{D2} = 350$ nM (solid line), $K_{D1} = K_{D2} = 13$ nM (dotted line), and $K_{D1} = K_{D2} = 350$ nM (dashed line).

visual inspection as well as goodness-of-fit values. Table 1 shows the results of comparable fits to the experimental data obtained in titrations of 16:0- and 17:0-dACPs.

Mass Balance Evaluation. Figure 5 shows plots of the concentrations of the three enzyme species indicated in Figure 2 as given by NSolve solutions at various concentrations of 18:0-ACP and Δ9D. These plots were generated assuming $K_{D1} = 13$ nM and $K_{D2} = 350$ nM as determined from the experiments of Figure 4. The inset to each plot shows the species distribution expected when the total Δ9D concentration was in the range of 10−100 nM, which is relevant to the results of Figure 6 presented below. These plots reveal changes in the distribution of E_2, AE_2, and AE_2A that are useful in the evaluation of a variety of different experiments.

Figure 5A shows the species distribution calculated for a titration containing 3000 nM 18:0-ACP. This represents a typical concentration of 18:0-ACP in a steady-state kinetic assay and is comparable to the K_M value measured by GC/MS (*17*) and at high concentrations of radiolabeled 18:0-ACP (*31*). In the early stages of this titration, particularly at

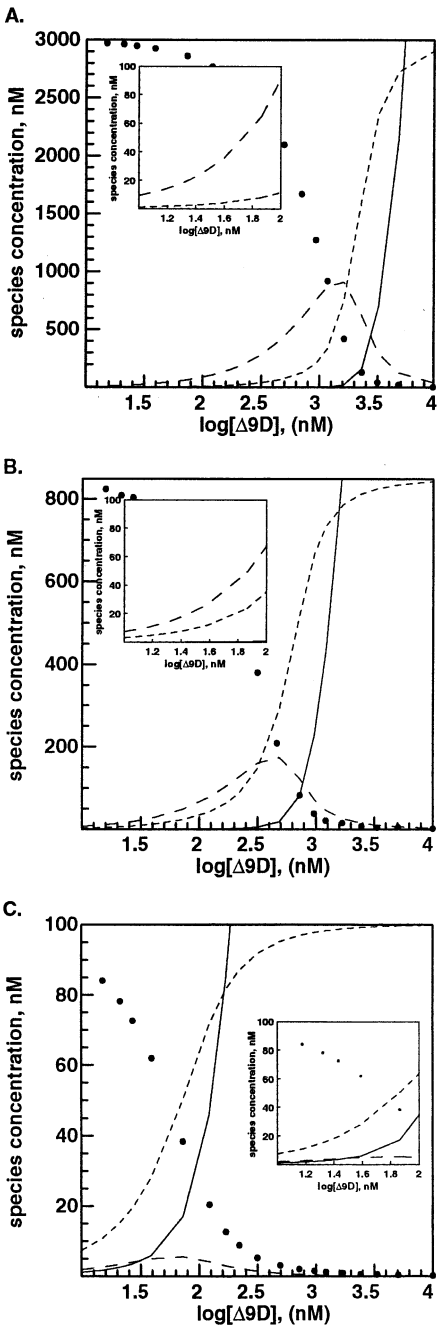

FIGURE 5: Concentrations of individual species present in titrations of 18:0-dACP with resting Δ9D as given by the NSolve solution of eqs 4−7 with $K_{D1} = 13$ nM and $K_{D2} = 350$ nM. In each plot, the solid line represents the concentration of E_2, the short dashed line represents the concentration of AE_2, the long dashed line represents the concentration of AE_2A, and the solid circles represent the concentration of free 18:0-ACP. The insets show expanded *y*-axes for the titration data from 1 to 100 nM added Δ9D. Some solid circles are covered by the insets; however, the general trend of changes in the concentration of free 18:0-ACP is still readily apparent. (A) Titration containing total 18:0-dACP of 3 μM. (B) Titration containing total 18:0-ACP of 850 nM. (C) Titration containing total 18:0-ACP of 100 nM.

the concentrations typical of steady-state catalytic assays (inset to Figure 5A, 20 nM Δ9D), AE_2A predominated until the concentration of E_2 achieved ~70% of the initial substrate concentration. After this point, the species distribution shifted rapidly to become dominated by AE_2, as the high-affinity site in the newly added E_2 effectively competed for 18:0-

ACP already bound to AE_2A. An overall similar species distribution is shown in Figure 5B, calculated for a titration containing 850 nM 18:0-ACP. This calculation corresponds to the concentration of 18:0-dACP used for the titration experiments of Figure 4. In this case, the dominant solution equilibrium initially involved conversion between AE_2 and AE_2A until the concentration of added Δ9D exceeded ~320 nM. Above this concentration, the dominant solution equilibrium shifted to an interconversion between E_2 and AE_2.

Figure 5C shows the species distribution calculated for a titration containing 100 nM 18:0-ACP. This corresponds to the concentration of 18:0-fACP present in the rapid-mix experiments of Figure 6 (see below) and is also comparable to the K_M value measured by a radioisotopic method at low 18:0-ACP concentrations (*19*, *32*). Unlike the titrations of Figure 5A,B, all stages of this titration involved a dominant solution equilibrium between E_2 and AE_2 because of the limiting amount of 18:0-ACP present.

Determination of Dissociation Rate Constants. Figure 6 shows the time-dependent anisotropy changes resulting from the dissociation of 16:0-, 17:0-, and 18:0-fACP from Δ9D. The results from control experiments where the different preformed acyl-fACP·Δ9D complexes were mixed with buffer are also shown. Due to detection limits required for the stopped-flow experiments (~100 nM acyl-fACP), the predicted initial species distribution consisted of 12% E_2, 72% AE_2, and 16% AE_2A (Figure 5C). Moreover, the concentration of unlabeled 18:0-ACP required for effective competition (~10 μM) indicated that the end point of the experiment would correspond to the essentially complete conversion to AE_2A.

For each acyl-fACP complex investigated, a decrease in anisotropy was observed upon mixing with unlabeled 18:0-ACP, corresponding to the competitive displacement of the bound fluorophoric substrate by the unlabeled substrate. In each case, the data were well fitted by a single-exponential decay as judged by plotting residuals for the fits. The dissociation rate constants (k_{off}) calculated for the various acyl-fACPs from these fits are given in Table 1. An increase in k_{off} was observed as the length of the acyl chain attached to fACP was shortened, with an ~130-fold increase in k_{off} observed for 16:0-fACP as compared to 18:0-fACP. Furthermore, the end point anisotropy observed after the stopped-flow mixed solution had reached equilibrium was lower for 16:0-fACP relative to 17:0-fACP or, more noticeably, for 18:0-fACP. This difference in amplitude reflected the ability of the fixed, final concentration of unlabeled 18:0-ACP to more effectively compete against the less tightly bound 16:0- and 17:0-fACPs than the more tightly bound 18:0-fACP.

Effect of [2Fe-2S] Ferredoxin or Ionic Strength on Acyl-ACP and Resting Δ9D Binding. Figure 7A shows that the inclusion of oxidized Fd (solid circle symbols) in the titration buffer at the same concentration used for steady-state kinetic analysis (3 μM) had no effect on the K_{D1} values determined by titration of 18:0-fACP with Δ9D in the nanomolar concentration range. Furthermore, the inclusion of Fd did not change the nature of the electrostatic binding interaction observed when the Δ9D concentration was greater than ~5 μM. Figure 7B shows that the binding affinity of 18:0-fACP for Δ9D in the presence of 0.2 M NaCl was decreased only ~5-fold in the nanomolar concentration range ($K_{D1} = 37 \pm$

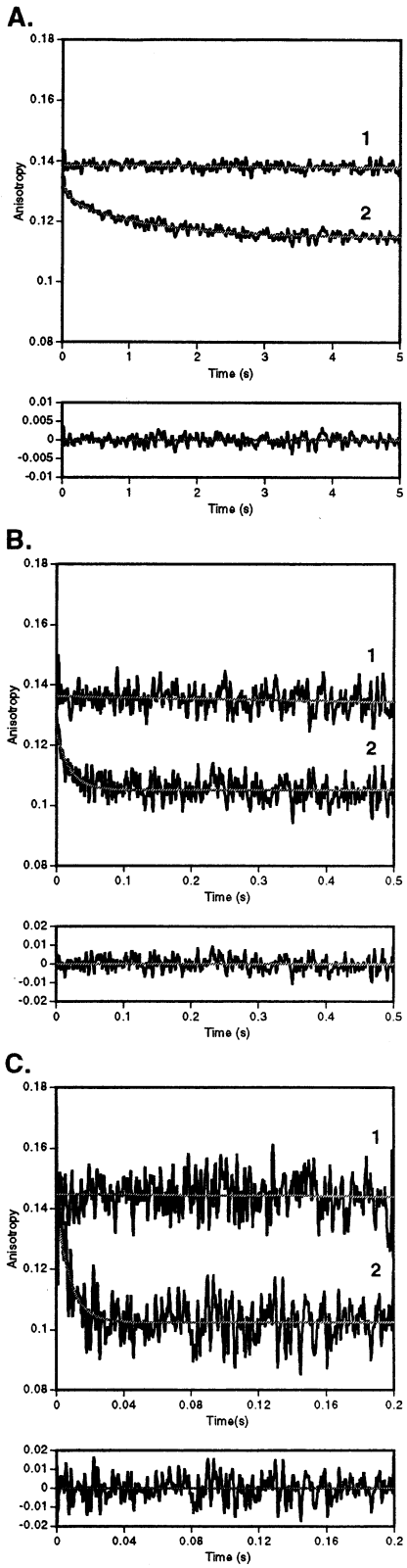

FIGURE 6: Dissociation of acyl-fACPs detected by time-dependent changes in fluorescence anisotropy after stopped-flow mixing with (1) buffer or (2) nonlabeled 18:0-ACP. The solid lines are the result of (1) linear or (2) single-exponential least-squares fitting. The residuals for the single-exponential fits are shown in the panels below the experimental data. (A) 18:0-fACP−Δ9D complex and a 5 s data collection period. (B) 17:0-fACP−Δ9D complex and a 0.5 s data collection period. (C) 16:0-fACP−Δ9D complex and a 0.2 s data collection period The decrease in signal-to-noise ratio in experiments with a shorter data collection time was due to time-dependent changes in the oversampling rate.

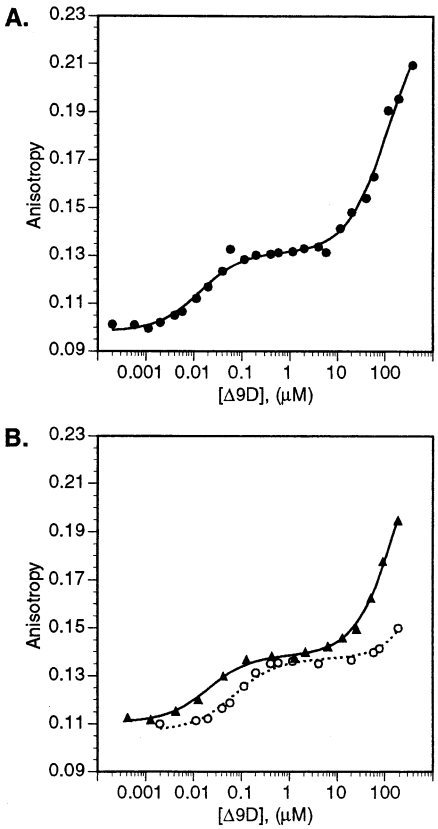

FIGURE 7: Fluorescence anisotropy changes observed during titration of 1 nM 18:0-fACP with Δ9D at pH 7.8 in the presence of (A) (●) 3 μM [2Fe-2S] Fd and (B) either (▲) 0.035 M NaCl or (○) 0.2 M NaCl. Solid and dotted lines were obtained as described in the caption to Figure 1.

7.7 nM) as compared to the K_{D1} determined in the presence of 35 mM NaCl. In contrast, the change in anisotropy assigned to nonspecific electrostatic interactions was nearly completely eliminated ($K_{non} > 500$ μM). When steady-state kinetic measurements were performed in buffer modified to include 0.2 M NaCl, only a slight increase in k_{cat} was observed (0.65 s^{-1}) relative to the assay buffer containing 35 mM NaCl (0.55 s^{-1}).

DISCUSSION

The utility of fluorescence anisotropy for the study of binding interactions of proteins, nucleic acids, and various ligands is now well established (*23*, *33*, *34*). To our knowledge, this work represents the first use of fluorescence anisotropy to study the participation of an acyl carrier protein in enzyme complex formation. This experimental approach has permitted a dynamic investigation of binding interactions over an ~10^4 range of enzyme and substrate concentrations. Due to the participation of ACPs in many other important biological reactions (*35*), this labeling strategy may provide a broadly applicable basis for other types of steady-state and time-resolved anisotropy measurements.

Binding Equilibria. Due to mass balance considerations inherent in the experimental design required for anisotropy measurements, the titration of ~1 nM *n*:0-fACPs with Δ9D most accurately assessed the binding equilibrium assigned to K_{D1} in Figure 2. In contrast, the titration of ~850 nM *n*:0-fACPs provided an estimate for the K_{D2} value associated with saturation of both binding sites on dimeric Δ9D (Figure 2). These results suggest that the tightly bound forms associated with AE_2 and AE_2A (forms present at the Δ9D and *n*:0-ACP concentrations of the assay) are likely most relevant to catalysis. The ability to measure two different K_D values arose in part from the difference in fluorescence quantum yield for the two probes utilized, which allowed similar experiments to be performed in ACP concentration regimes differing by 850-fold. Furthermore, these measurements were possible because neither probe experienced changes in quantum yield during the respective titrations. This indicates that both probes experience similar environments when either free or bound.

Here we have shown that formation of the AE_2 complex is associated with an ~4-fold increase in affinity per methylene group and that formation of the AE_2A complex is associated with an ~2-fold increase in affinity per methylene group (Table 1). Assuming two identical and independent sites in dimeric Δ9D and the statistical factors accounting for different intermediate microscopic complexes, $K_{D2} = 4K_{D1}$ (*36*). However, the K_{D1} value of 13 nM represents a distinct, approximately 30-fold tighter binding equilibrium than the K_{D2} value of ~350 nM. This difference in affinities for the first and second binding events provides experimental evidence that resting Δ9D exhibits negative cooperativity for substrate binding in the conversion from AE_2 to AE_2A. Examination of the X-ray structure of the substrate-free reduced enzyme (*12*) suggests that extensive interactions between the acyl-ACP (~9 kDa) and Δ9D (~42 kDa subunit) will likely be produced upon substrate binding. Hence, it is reasonable that conformational adjustments induced by formation of AE_2 could influence subsequent conversion to AE_2A.

Electrostatic Contributions to the ES Complex. High concentrations of Δ9D (greater than 5 μM, Figure 3) resulted in the formation of an electrostatic complex, presumably between the already formed AE_2 and excess E_2. Since the surface of Δ9D contains an abundance of Arg and Lys residues near the opening of the putative active site channel (*12*), and since *E. coli* ACP has an abundance of surface Asp and Glu residues (*37*), there is a significant potential for nonphysiological electrostatic interactions. These electrostatic interactions could be largely eliminated by the inclusion of 0.2 M NaCl in the sample buffers, which had only minimal consequences on catalytic turnover. Moreover, the small increase in k_{cat} observed at high ionic strength is consistent with the proposal that hydrophobic binding provides an important input to catalysis (*17*).

Mass Balance Evaluation. The measured K_D values allowed a calculation of the enzyme species predicted to be present under various experimental conditions. For our typical catalytic assays, a predominance of the AE_2A form was predicted when 18:0-ACP exceeded ~850 nM (Figure 5B). However, as the 18:0-ACP concentration was decreased, the AE_2 form began to dominate, and catalytic turnover with an 18:0-ACP concentration of 100 nM would proceed with AE_2 as the dominant species present (Figure 5C). Extension of these calculations to an evaluation of other experiments, such as spectroscopic studies of well-characterized peroxo-Δ9D, indicates the complete conversion of all Δ9D to AE_2A, which is consistent with the observed spectroscopic homogeneity (*14*, *16*).

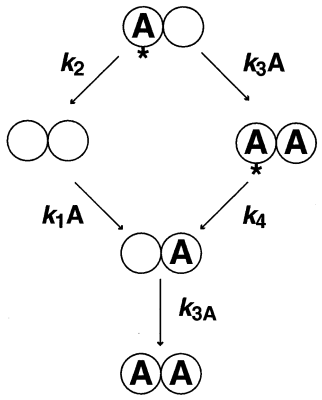

FIGURE 8: Binding equilibria corresponding to potential reactions observed during the rapid-mix dissociation of acyl-ACPs shown in Figure 6. A*, labeled *n*:0-ACP substrate; A, *n*:0-ACP substrate.

Dissociation Constant for the ES Complex. Figure 6 provides experimental evidence that the stability of the various enzyme−substrate complexes may provide a major input to the catalytic selectivity of Δ9D for 18:0-ACP relative to 16:0-ACP. The high quality of the single-exponential fits shown in Figure 6 indicates that a unimolecular relaxation event has been measured. Within the constraints established by the mass balance analysis reported above (72% of AE_2 initially present) and the stoichiometric accumulation of AE_2A at the end point as a consequence of the high concentration of unlabeled 18:0-ACP added at the rapid mix, three different origins of the unimolecular relaxation can be considered. Figure 8 provides a schematic representation of the binding equilibria potentially involved. First, k_2 and k_4 of Figure 2 may be equivalent within experimental error, which implies that k_1 and k_3 must differ by ∼30-fold at equal substrate concentrations in order to account for the overall negative cooperativity revealed by the measured differences in K_{D1} and K_{D2}. Second, k_2 may greatly exceed the second-order rate constant given by k_3A at experimental concentrations, so that the release of bound *n*:0-fACP would be faster than the pseudo-first-order binding of excess 18:0-ACP introduced upon rapid mixing. In this case, the measured relaxation would correspond uniquely to k_2. Third, k_3A may greatly exceed k_2 at experimental conditions, resulting in an initial rapid conversion to a mixed A^*E_2A complex. In this case, the measured relaxation rate would correspond to k_4 as A* was replaced by A in the final AE_2A complex. A conclusive discrimination between these three options is not possible with the presently available data. Nevertheless, calculations using the measured k_{off} and K_D values result in bimolecular association rates $\sim 10^2-10^3$-fold slower than the diffusion limit. This is consistent with the large molecule nature of the substrate involved as well as the possible contributions of conformational rearrangements and other postcollision aspects of the binding interaction.

Implications for the Δ9D Catalytic Cycle. The use of fluorescence anisotropy to measure equilibrium binding interactions has provided a new and more detailed view of the role of interactions between the 18:0-ACP and Δ9D in soluble desaturase catalysis. The present work substantially refines the accumulating evidence that substrate binding interactions provide important determinants of Δ9D catalysis. Here we have demonstrated that the length of the acyl chain is associated with the stability of the enzyme−substrate complex. This correlation is strongly indicative that the catalytic selectivity of Δ9D may derive in major part from a partition between dissociation of the enzyme−substrate complex and subsequent steps leading to chemistry (*38*, *39*). This interplay of k_{off} with subsequent reaction steps for the AE_2A complex is now a matter of current investigation.

ACKNOWLEDGMENT

We thank Prof. E. Craig (Department of Biomolecular Chemistry) and Prof. G. Roberts (Department of Bacteriology) for access to their Beacon 2000 spectrophotometers during this work. We also thank Prof. E. Chapman (Department of Anatomy) for use of his stopped-flow spectrofluorometer and Mr. J. Bai for expert assistance. J.A.H. and B.G.F. acknowledge many helpful discussions with Dr. J. Gross, Dr. A. Hegeman, Prof. W. W. Cleland, and Prof. D. B. Northrop.

REFERENCES

1. Nagai, J., and Bloch, K. (1968) *J. Biol. Chem. 243*, 4626−4633.
2. Redenbach, M., Kieser, H. M., Denapaite, D., Eichner, A., Cullum, J., Kinashi, H., and Hopwood, D. A. (1996) *Mol. Microbiol. 21*, 77−96.
3. Cole, S. T., Brosch, R., Parkhill, J., Garnier, T., Churcher, C., Harris, D., Gordon, S. V., Eiglmeier, K., Gas, S., Barry, C. E., III, Tekaia, F., Badcock, K., Basham, D., Brown, D., Chillingworth, T., Connor, R., Davies, R., Devlin, K., Feltwell, T., Gentles, S., Hamlin, N., Holroyd, S., Hornsby, T., Jagels, K., Barrell, B. G., et al. (1998) *Nature 393*, 537−544.
4. Fox, B. G., Shanklin, J., Somerville, C., and Münck, E. (1993) *Proc. Natl. Acad. Sci. U.S.A. 90*, 2486-2490.
5. van de Loo, F. J., Fox, B. G., and Somerville, C. (1993) in *Lipid Metabolism in Plants* (Moore, T. E., Ed.) pp 91−126, CRC Press, Boca Raton, FL.
6. Fox, B. G., Shanklin, J., Ai, J., Loehr, T. M., and Sanders-Loehr, J. (1994) *Biochemistry 33*, 12776−12786.
7. Fox, B. G. (1998) in *Comprehensive Biological Catalysis* (Sinnott, M., Ed.) pp 261−348, Academic Press, London.
8. Ryle, M. J., and Hausinger, R. P. (2002) *Curr. Opin. Chem. Biol. 6*, 193−201.
9. Nordlund, P., and Eklund, H. (1995) *Curr. Opin. Struct. Biol. 5*, 758−766.
10. Merkx, M., Kopp, D. A., Sazinsky, M. H., Blazyk, J. L., Muller, J., and Lippard, S. J. (2001) *Angew. Chem., Int. Ed. Engl. 40*, 2782−2807.
11. Solomon, E. I., Brunold, T. C., Davis, M. I., Kemsley, J. N., Lee, S.-K., Lehnert, N., Neese, F., Skulan, A. J., Yang, Y.-S., and Zhou, J. (2000) *Chem. Rev. 100*, 235−349.
12. Lindqvist, Y., Huang, W., Schneider, G., and Shanklin, J. (1996) *EMBO J. 15*, 4081−4092.
13. Shu, L., Broadwater, J. A., Achim, C., Fox, B. G., Münck, E., and Que, L., Jr. (1998) *J. Biol. Inorg. Chem. 3*, 392−400.
14. Broadwater, J. A., Ai, J., Loehr, T. M., Sanders-Loehr, J., and Fox, B. G. (1998) *Biochemistry 37*, 14664−14671.
15. Yang, Y.-S., Broadwater, J. A., Fox, B. G., and Solomon, E. I. (1999) *J. Am. Chem. Soc. 121*, 2770−2783.
16. Broadwater, J. A., Achim, C., Münck, E., and Fox, B. G. (1999) *Biochemistry 38*, 12197−12204.
17. Haas, J. A., and Fox, B. G. (1999) *Biochemistry 38*, 12833−12840.
18. Lyle, K. S., Ai, J., Moenne-Loccoz, P., Sanders-Loehr, J., Loehr, T. M., and Fox, B. G. (2000) *Biochemistry 39*, 10507−10513.
19. Whittle, E., and Shanklin, J. (2001) *J. Biol. Chem. 276*, 21500−21505.
20. Haas, J. A., Frederick, M. A., and Fox, B. G. (2000) *Protein Expression Purif. 20*, 274−284.
21. Hoffman, B. J., Broadwater, J. A., Johnson, P., Harper, J., Fox, B. G., and Kenealy, W. R. (1995) *Protein Expression Purif. 6*, 646−654.
22. Haugland, R. P. (1996) in *Handbook of Fluorescent Probes and Research Chemicals*, 6th ed., p 679, Molecular Probes, Eugene, OR.

23. Lakowicz, J. R. (1999) in *Principles of Fluorescence Spectroscopy*, 2nd ed., Kluwer Academic/Plenum Publishers, New York.
24. Mendel, C. M., and Mendel, D. B. (1985) *Biochem. J. 228*, 269−272.
25. Abita, J. P., Lzdunski, M., and Ailhaud, G. P. (1971) *Eur. J. Biochem. 23*, 412−420.
26. Prescott, D. J., and Vagelos, P. R. (1972) *Adv. Enzymol. 36*, 269−311.
27. Broadwater, J. A., and Fox, B. G. (1998) *Protein Expression Purif. 15*, 314−326.
28. Holak, T. A., Kearsley, S. K., Kim, Y., and Prestegard, J. H. (1988) *Biochemistry 27*, 6135−6142.
29. Danliker, W. B., Hsu, M.-L., Levin, J., and Rao, B. R. (1981) *Methods Enzymol. 74*, 3−28.
30. Lunblad, J. R., Laurance, M., and Goodman, R. H. (1996) *Mol. Endocrinol. 10*, 607−612.
31. Gibson, K. J. (1993) *Biochim. Biophys. Acta 1169*, 231−235.
32. McKeon, T. A., and Stumpf, P. K. (1982) *J. Biol. Chem. 257*, 12141−12147.
33. Heyduk, T., Ma, Y., Tang, H., and Ebright, R. H. (1996) *Methods Enzymol. 274*, 492−505.
34. Hill, J. J., and Royer, C. A. (1997) *Methods Enzymol. 278*, 390−416.
35. Heath, R. J., White, S. W., and Rock, C. O. (2001) *Prog. Lipid Res. 40*, 467−497.
36. Segel, I. H. (1975) in *Enzyme Kinetics*: *Behavior and Analysis of Rapid Equilibrium and Steady-State Enzyme Systems*, p 957, John Wiley and Sons, New York.
37. Kim, Y., and Prestegard, J. (1990) *Proteins*: *Struct., Funct., Genet. 8*, 377−385.
38. Northrop, D. B. (1977) in *Isotope Effects on Enzyme-Catalyzed Reactions* (Cleland, W. W., O'Leary, M., and Northrup, D. B., Eds.) pp 122−157, University Park Press, Baltimore, MD.
39. Northrop, D. B. (1999) in *Enzymatic Mechanisms* (Frey, P. A., and Northrop, D., Eds.) pp 250−263, IOS Press, Amsterdam.

BI020340S